Journal of Sound and Vibration 471 (2020) 115199

Contents lists available at ScienceDirect

Journal of Sound and Vibration

journal homepage: www.elsevier.com/locate/jsvi

Interpretation of the Acoustic Black Hole effect based on the concept of critical coupling

J. Leng [a,*], V. Romero-García [a], A. Pelat [a], R. Picó [b], J.-P. Groby [a], F. Gautier [a]

[a] Laboratoire d'Acoustique de l'Université du Mans, LAUM, UMR CNRS 6613, Av. Olivier Messiaen, Le Mans, France
[b] Instituto para la Gestión Integral de Zonas Costeras (IGIC), Universitat Politècnica de València, Paranimf 1, 46730, Gandia, Spain

ARTICLE INFO

Article history:
Received 27 June 2019
Revised 13 January 2020
Accepted 15 January 2020
Available online 19 January 2020
Handling Editor: J Cheer

Keywords:
Vibration damper
Acoustic Black Hole effect
Reflection coefficient
Critical coupling

ABSTRACT

An Acoustic Black Hole (ABH) in a one-dimensional (1D) beam is a passive vibration damping device based on a local reduction of the beam thickness attached to a thin layer of attenuating material. This work aims at revisiting the ABH effect by analysing the ABH trapped modes in the complex frequency plane. This analysis relies on an analytical model based on the one-dimensional thin beam theory and the transfer matrix method which assumes that the ABH termination is discretised by constant thickness piecewise elements. The model is validated with numerical simulations by the Finite Element Method. The reflection coefficients of several ABH terminations are studied. The results show that an ABH presents an infinite number of modes associated to an infinite number of poles and zeros of the reflection coefficient, the density and quality factor of which depend on the order of the ABH profile. By considering the ABH termination as an open lossy resonator, its damping efficiency results therefore from a balance between the energy leakage of each mode and its inherent losses, known as the critical coupling condition. In particular, the broadband absorption of the vibration energy is achieved for frequencies higher than that of the mode that is critically coupled. This type of analysis is used to interpret the ABH effect. It provides the losses needed to obtain the critical coupling condition, and is suitable for the optimisation of one-dimensional ABH terminations.

1. Introduction

Vibration damping of mechanical structures at low frequencies is a crucial issue in terms of safety, stability, and comfort in many industrial applications. The usual passive way to solve this problem relies on the use of viscoelastic coatings [1]. In this case, the vibration damping results from heat dissipation obtained by the shear forces in the viscoelastic material. Nevertheless, this solution may be accompanied by a significant increase in the weight of the structure which becomes inconvenient for practical, ecological and economic reasons. The use of the Acoustic Black Hole (ABH) is therefore particularly relevant in this context. The ideal implementation of an ABH in a one-dimensional (1D) beam consists of continuously decreasing the thickness of the beam according to a power-law until it vanishes [2]. As a result, the flexural wave slows down by propagating along the termination until reaching zero phase and group velocities at its extremity. The wave is therefore not reflected and an anechoic termination is obtained. However, in practice the thickness profile must be truncated. This leads to a non-null thickness at its tip and therefore to a total reflection of the flexural waves in the absence of loss. However, losses are not avoidable, and the combination of the ABH effect with damping devices has been proposed in the form of spiral ABHs [3], compound ABHs [4],

* Corresponding author.
E-mail address: julien.leng@univ-lemans.fr (J. Leng).

https://doi.org/10.1016/j.jsv.2020.115199
0022-460X/

and ABH resonant beam dampers [5], to cite a few. Other applications such as insulating [6] and lensing [7,8] devices have been also proposed, as well as strategies to enhance the ABH performance. These strategies include the use of extended platforms [9], passive constrained layers [10] or exploit beam non-linearities [11,12].

Recently, the representation of the eigenvalues of the scattering matrix in the complex frequency plane has been exploited to interpret and design perfect absorbers [13,14]. In the case of a locally resonant termination, an ABH termination for instance, the reflection coefficient represents the scattering matrix which is scalar in this kind of problem. As a consequence, the reflection coefficient is the eigenvalue of the problem. It has been shown that the reflection coefficient presents pairs of zeros and poles in the complex frequency plane [13,14]. These zeros and poles are complex conjugates one with respect to the other in the lossless case, thus they are symmetric with respect to the real frequency axis. In the ideal case of an ABH in which the thickness is zero, the reflection coefficient should present a continuous number of poles and zeros that coalesce at the real frequency axis. However, this situation is not realistic since the thickness, despite its small value, is nonetheless always finite. In this case, infinite discrete symmetric pairs of poles and zeros appear in the complex frequency plane. At this stage, it is worth noting that the imaginary part of the pole represents the energy leakage from the ABH tip to the main beam as this kind of termination can be interpreted as an open resonator [14].

The damping efficiency of these open resonators can be improved by making use of the inherent losses of the system. In doing so, the zeros and poles can be tuned in the frequency plane by taping a layer of viscoelastic material along the thickness profile [14] for instance. Thus, the pairs of zeros/poles move along the imaginary frequency axis in the same direction as the loss increases, locating the zeros closer to the real frequency axis [13,14]. In particular, perfect absorption of the incident wave can be achieved when a zero is located on the real frequency axis. In other words, when the energy leakage is perfectly compensated by the added losses. This corresponds to the critical coupling condition [15], and has been widely used to design perfect absorbers in various fields of wave physics [16–18]. Concurrently, it has been shown that the damping efficiency of a practical ABH, also called ABH effect, can be significantly improved by adding a thin layer of viscoelastic material along the ABH profile [19,20]. The reflection coefficient of such a system has been studied both experimentally [21] and numerically by using various methods: plane wave decompositions [22] or multimodal approaches [23], Finite Difference [24] or Finite Element [25] methods, and wavelet decompositions [26], to cite a few. In general, the ABH effect is characterised by a falling reflection coefficient at specific frequencies corresponding to modes of the tapered zone [24]. However, it has not been shown in detail how the losses should be managed to obtain the perfect absorption of flexural waves.

This article focuses on the link between the complex nature of the trapped modes within a 1D ABH and the drops in its reflection coefficient, in terms of depth and frequency width. More specifically, the purpose of the present article is to analyse first the absorbing efficiency of the ABH by using the critical coupling condition. The absorption of the ABH termination can be controlled by tuning the losses introduced via the added viscoelastic coating and the geometry of the ABH. Two strategies to optimise the absorption efficiency of an ABH termination at low frequency are then proposed in this work, both consisting in applying the critical coupling condition. The first of these strategies consists in tuning the losses introduced by the viscoelastic layer by shaping its thickness profile in order to achieve the critical coupling condition at several resonances of the ABH. The second strategy is based on the addition of a mass at the extremity of the ABH which decreases the first resonance frequency of the ABH. The critical coupling is then applied at this specific frequency to obtain a low frequency absorption by the termination.

The analysed system is composed of a main beam terminated by an open resonator which corresponds to an ABH of finite length. The ABH termination is discretised by constant thickness piecewise elements. A thin viscoelastic coating is also attached to the ABH creating a composite material. This composite material is modeled with the Ross-Kerwin-Ungar (RKU) method [1]. The vibration response of the composite ABH is studied by means of the transfer matrix method (TMM) [27]. In particular, the eigenvalue of the scattering matrix S for the propagating waves are analysed in the complex frequency plane [13,14], providing insightful interpretations on the absorption efficiency of the ABH. All the analytical results are validated with full wave numerical simulations by Finite Element Models, which have been implemented using 2D models of solid mechanics in COMSOL Multiphysics software.

The work is organised as follows. In Section 2, the theoretical model used to analyse the reflection of flexural waves by a profiled termination is presented for a 1D reflection problem. In Section 3, the physical interpretations of the ABH effect of a truncated ABH with a coating layer are presented by using the complex frequency plane in the lossless and lossy cases. Section 4 proposes two strategies to optimise the absorption efficiency of an ABH termination at low frequency. The first consists in tuning the losses introduced by the added coating layer in order to apply the critical coupling condition. The second strategy consists in adding a mass at the end of the ABH in order to introduce a degree of freedom in the low frequency regime, where the ABH is not efficient. All the analytical results are validated with a numerical model using the finite element formalism. Finally, Section 5 summarises the main results and gives the concluding remarks.

2. Theoretical model for the reflection of flexural waves by a profiled termination

This Section describes the theoretical model used to study the absorption of flexural waves by a 1D open, lossy, and profiled termination. The model is based on the TMM as proposed by Mace [27] and previously used to interpret the perfect absorption of flexural waves by a termination composed of a thin beam with a uniform thickness [14]. This method is applied here to compute the reflection coefficient of finite beam terminations described by $N-1$ piecewise constant property profiles, as depicted in Fig. 1.

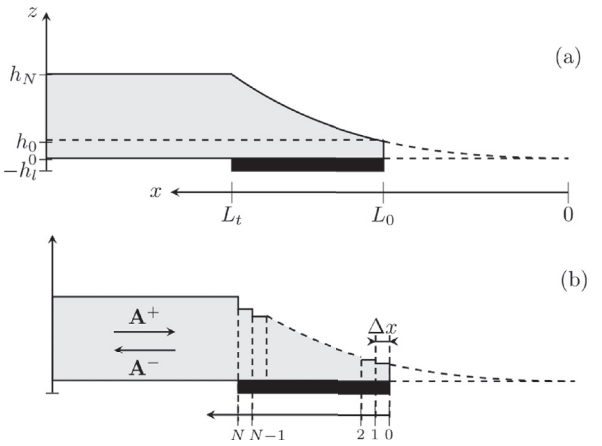

Fig. 1. (a) Diagrams of the 1D reflection problem for flexural waves. (b) Spatial discretisation of the thickness profile of the ABH termination.

2.1. Reflection problem

Consider a time harmonic ($e^{i\omega t}$) incident plane wave that impinges the ABH termination from the left (see Fig. 1(a)). The ABH is discretised into $N-1$ beams of identical length Δx, but of height h_j, bending stiffness $D_j = EI_j$ where $I_j = bh_j^3/12$ denotes the second moment of area, b being the beam width, and wavenumbers $k_j^4 = \frac{\rho_j b h_j \omega^2}{D_j}, j = 0, \ldots, N$ where bh_j is the cross-sectional area of segment j (see Fig. 1(b)). The material of the main beam and the uncoated ABH termination is identical, with E its Young's modulus and ρ its mass density. The losses are accounted for via a loss factor η, the complex Young's modulus thus being $E(1+i\eta)$. The possible variations of the loss factor with the frequency are ignored in this study, and η is assumed to be constant. This assumption is reasonable in the case of the aluminium beam studied in this work. The continuity and equilibrium of the displacement, slope, bending moment and shear force are considered at the interfaces between each consecutive beam. Assuming the Euler-Bernoulli conditions, the flexural displacement $\mathbf{W}$ in the main beam, i.e. for $x > L_t$, reads as

$$\mathbf{W} = \mathbf{A}^+ + \mathbf{A}^- = \left(\mathbf{I} + \mathbf{R_N}\right)\mathbf{A}^+, \tag{1}$$

where $\mathbf{A}$ represents the complex amplitude vectors of the propagative and evanescent waves, the signs $^+$ and $^-$ denote the ingoing and outgoing waves respectively, $\mathbf{R_N}$ is the reflection matrix at $x = L_t$, i.e. at the interface between the main beam and the ABH termination, and $\mathbf{I}$ is the identity matrix.

The expression of $\mathbf{R_N}$ is a combination of reflection and transmission matrices at the interfaces of all the discrete beams that form the termination. It is obtained iteratively starting from the reflection matrix of the free termination $\mathbf{R_0} = \mathbf{R_{free}}$ given by

$$\mathbf{R_{free}} = \begin{bmatrix} -i & (1+i) \\ (1-i) & i \end{bmatrix}. \tag{2}$$

The iterative scheme takes the following form [27].

$$\mathbf{R_j} = \mathcal{R}_{\mathbf{j-1,j}} + \mathcal{T}_{\mathbf{j-1,j}}\left[(\mathbf{F_{j-1}}\mathbf{R_{j-1}}\mathbf{F_{j-1}})^{-1} - \mathcal{R}_{\mathbf{j,j-1}}\right]^{-1}\mathcal{T}_{\mathbf{j,j-1}}, \text{for } j = 1 \text{ to } N, \tag{3}$$

where $\mathcal{R}_{\mathbf{i,j}}$ and $\mathcal{T}_{\mathbf{i,j}}$ are the reflection and transmission matrices from section i to section j respectively. Considering the continuity and equilibrium of the displacement, slope, bending moment and shear force, these matrices are given by

$$\mathcal{T}_{\mathbf{ij}} = \frac{4}{\Delta_{ij}}\begin{bmatrix} (1+\beta_{ij})(1+\gamma_{ij}) & (-1+i\beta_{ij})(1-\gamma_{ij}) \\ (-1-i\beta_{ij})(1-\gamma_{ij}) & (1+\beta_{ij})(1+\gamma_{ij}) \end{bmatrix}, \tag{4}$$

$$\mathcal{R}_{\mathbf{ij}} = \frac{2}{\Delta_{ij}}\begin{bmatrix} -2(\beta_{ij}^2-1)\gamma_{ij} - i\beta_{ij}(1-\gamma_{ij})^2 & (1+i)\beta_{ij}(1-\gamma_{ij}^2) \\ (1-i)\beta_{ij}(1-\gamma_{ij}^2) & -2(\beta_{ij}^2-1)\gamma_{ij} + i\beta_{ij}(1-\gamma_{ij})^2 \end{bmatrix}, \tag{5}$$

where $\beta_{ij} = \frac{k_j}{k_i}$ and $\gamma_{ij} = \frac{D_j k_j^2}{D_i k_i^2}$ correspond to the ratios of wavenumbers and bending wave impedances, and $\Delta_{ij} = (1+\beta_{ij})^2(1+\gamma_{ij})^2 - (1+\beta_{ij}^2)(1-\gamma_{ij})^2$. The diagonal transfer matrix $\mathbf{F_j}$ in the uniform beams is expressed as

$$\mathbf{F_j} = \begin{bmatrix} e^{-ik_j x} & 0 \\ 0 & e^{-k_j x} \end{bmatrix}. \tag{6}$$

Table 1
Geometric and material parameters of the studied systems. The value of the loss factors η and η_l depends on the experimental set-up used. The parameter b corresponds to the width of the system.

	Geometric parameters	Material parameters
Main beam	$h_N = 5$ mm $b = 2$ cm	$\rho = 2700$ kg m^{-3} $E = 70$ GPa η
Acoustic Black Hole	$h_0 = 0.1125$ mm $b = 2$ cm $L_t = 20$ cm $L_0 = 3$ cm $N = 201$	ρ_j D_j
Coating layer	$h_l = 0.7$ mm	$E_l = 0.5$ GPa $\rho_l = 950$ kg m^{-3} η_l

$\mathbf{R_N}$ is thus a 2×2 matrix where the upper diagonal component corresponds to the reflection coefficient of the propagative wave. The study focuses on the term $R_N \equiv \mathbf{R_N}(1,1)$ which is the only one related to the carried energy. Only $\mathbf{R_N}(1,1)$ and $\mathbf{R_N}(2,1)$ contribute to the reflected field in the abscence of evanescent incident waves. Moreover, $\mathbf{R_N}(2,1)$ vanishes in the far-field ($x \to -\infty$) as it corresponds to the converted waves from propagative to evanescent waves during the reflection process. As the configuration presented in this work corresponds to a reflection problem, no wave is transmitted by the termination. In this case, the scattering matrix collapses to a scalar which is the reflection coefficient. Therefore, the reflection coefficient R_N represents the scattering of the system and corresponds directly to both the scattering matrix of the termination and its associated eigenvalue. The absorption coefficient α_R can thus be written as:

$$\alpha_r = 1 - |R_N|^2, \qquad x \to \infty. \tag{7}$$

2.2. Introducing viscoelastic losses in the system: the RKU model

A thin viscoelastic layer of identical material, and constant thickness piecewise h_j^l is now added along the termination length as shown in Fig. 1. Each discretised element of the viscoelastic layer coincides with those of the ABH. The losses are assumed to be frequency independent and characterised by a Young's Modulus $E_l(1 + i\eta_l)$, where η_l is the loss factor of the viscoelastic material. Using the RKU model [1], the effective bending stiffness D_j^c of the j-th discretised composite beam of the tapered area is written as [22]:

$$D_j^c = EI_j \left\{ (1+i\eta) + e_c \widetilde{h}_c^3 (1+i\eta_l) + \frac{3 + (1+\widetilde{h}_c)^2 e_c h_c [1 - \eta\eta_l + i(\eta+\eta_l)]}{1 + e_c \widetilde{h}_c (1+i\eta_l)} \right\}, \tag{8}$$

where the indices j and l stand for the parameters of the uncoated j-th beam of the termination and the absorbing layer respectively, $e_c = E_l/E$ and $\widetilde{h}_c = h_j^l/h_j$. In addition, the wave number k_j^c of the j-th composite beam satisfies $(k_j^c)^4 = \frac{\rho_j^c b h_j^c \omega^2}{D_j^c}$, where $h_j^c = h_j^l + h_j$ is the total composite height and $\rho_j^c = (\rho_j h_j + \rho_l h_l)/h_j^c$ is the density.

3. Interpretation of the ABH effect by analysing R_N in the complex frequency plane

The absorption of flexural waves by a discretised 1D ABH termination onto which a viscoelastic layer has been added is now analysed in the reflection problem. In this section, the thickness h_j^l of the viscoelastic layer is considered constant such that $h_j^l = h_l$, for $j = 0, \ldots, N-1$. The eigenvalue of the scattering matrix of the propagative wave is reduced to R_N in the current case and is analysed in the complex frequency plane [13,14]. The material properties and geometric parameters are also given in Table 1.

3.1. Analysis of lossless ABH terminations with different thickness profiles

Four configurations of terminations with different thickness profiles of the uncoated ABH are analysed in this paragraph. The four thickness profiles differ from one another by their power-law χ, such that each profile equation reads as:

$$h(x) = h_N \left(\frac{x}{L_t} \right)^{\chi}, \forall x > L_0. \tag{9}$$

The analysed orders are linear ($\chi = 1$), quadratic ($\chi = 2$), cubic ($\chi = 3$) and quartic ($\chi = 4$) respectively and are depicted in Fig. 2(e). The reflection problem is analysed first for each configuration in the lossless case. In this case, no dissipation is

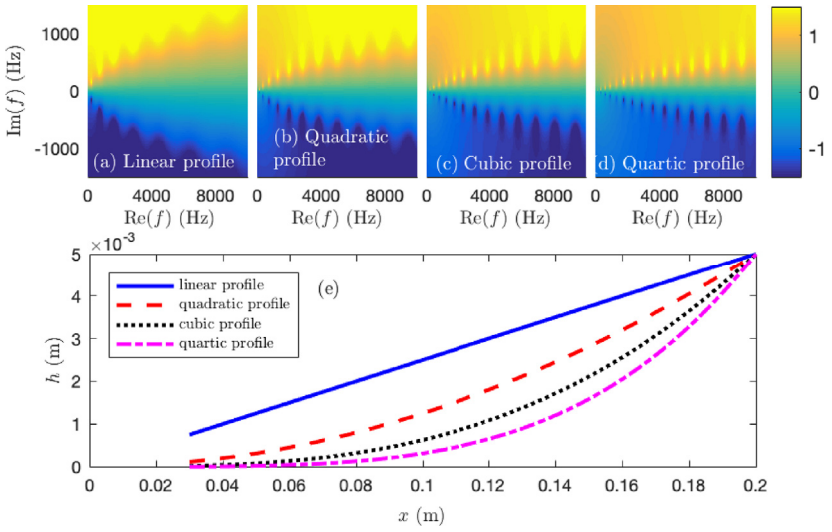

Fig. 2. (a)–(d) Representation of $\log_{10}(|R_N|)$ in the complex frequency plane for different thickness profiles of the ABH in the lossless case (linear, quadratic, cubic and quartic thickness profiles respectively). (e) Thickness profiles of the ABH studied in (a)–(d).

considered and the Young's moduli are pure real ($\eta = \eta_l = 0$). $\log_{10}(|R_N|)$ of the different thickness profiles are depicted in Fig. 2(a)–(d). For each profile order, the poles and zeros are symmetric by pair with respect to the real frequency axis in the lossless case, i.e. the complex frequencies associated to one pair of pole and zero are complex conjugate one from the other. This symmetric distribution comes from the time invariance symmetry of the scattering matrix [13]. The poles correspond to the resonances of the ABH termination while the zeros correspond to destructive interference phenomena. The value of $|R_N|$ along the real frequency axis is equal to 1 since no energy is lost in the system and the incoming wave is completely reflected back (see Fig. 2(d)). Since the ABH terminations are open resonators, the imaginary part of the poles in the lossless case represents the amount of energy leaked by the resonator through the main beam as previously shown in Ref. [13]. The quality factor of each resonance, and therefore of each pole, can be given by $Q = \frac{\mathrm{Re}(\omega_p)}{2\mathrm{Im}(\omega_p)}$ where ω_p corresponds to the complex frequency associated to the pole.

By observing the general trend of the discrete distribution of poles and zeros, it is possible to note that the imaginary part of the poles (and zeros) increases (decreases) when the real part of the frequency increases, meaning that more energy leaks out through the resonator when the frequency increases. As a consequence, the quality factor of the resonances also decreases as the frequency increases. Two different trends can also be observed according the thickness profiles. On the one hand, the density of poles increases with the order of the profile as shown in Fig. 2(a)–(d). On the other hand, the poles/zeros are closer to the real frequency axis as the order of the profile increases, meaning that the modes are more trapped in the termination and that the energy leakage is lower for higher profile orders. As a consequence, the quality factor Q of the modes increases with the order of the profile, leading to narrower poles and thus zeros.

The previous analysis corresponds to the lossless case. The next stage is to introduce losses in order to shift the zeros to the real frequency axis and design efficient absorbing devices. This situation corresponds to the critical coupling condition at which the introduced losses compensate the energy leakage of the system. Perfect absorption can therefore be observed in this case. In order to do this, a compromise between the density of poles and the quality factor must first be made in order to choose the proper profile. If a low (high) profile order is chosen, the density of poles will be low (high) and the quality factor will be low (high), requiring a big (low) amount of losses to produce a rippled reflection spectrum with broad (narrow) falling reflection. The quadratic profile is chosen here, with $\chi = 2$ which shows a reasonable density of poles with a leakage that can be compensated by realistic materials.

3.2. Lossy case

Losses are now introduced into the system. To do that, an imaginary part is added to the Young's modulus of the damping material of the viscoelastic coating such that it reads as $E_l(1 + i\eta_l)$. Losses in the uncoated termination and the main beam are neglected ($\eta = 0$). In doing so, the symmetry between the poles and zeros with respect to the real frequency axis is broken [13]. Fig. 3(b)-(c) depict $\log_{10}(|R_N|)$ in the complex frequency plane for two different values of η_l, which should be compared to the lossless case depicted in Fig. 3(a) ($\eta_l = 0$). As the losses induced by the damping layer increase ($\eta_l = 2$ in Fig. 3(b) and $\eta_l = 4$ in Fig. 3(c)), the zeros move to the real frequency axis. Falls of $|R|^2$ appear therefore in Fig. 3(d), and are associated to the resonance frequencies of the ABH termination. The closer to the real frequency axis the zero in the complex frequency plane, the greater the fall of $|R|^2$ with respect to the real frequency with two distinct situations: either the zeros are located in

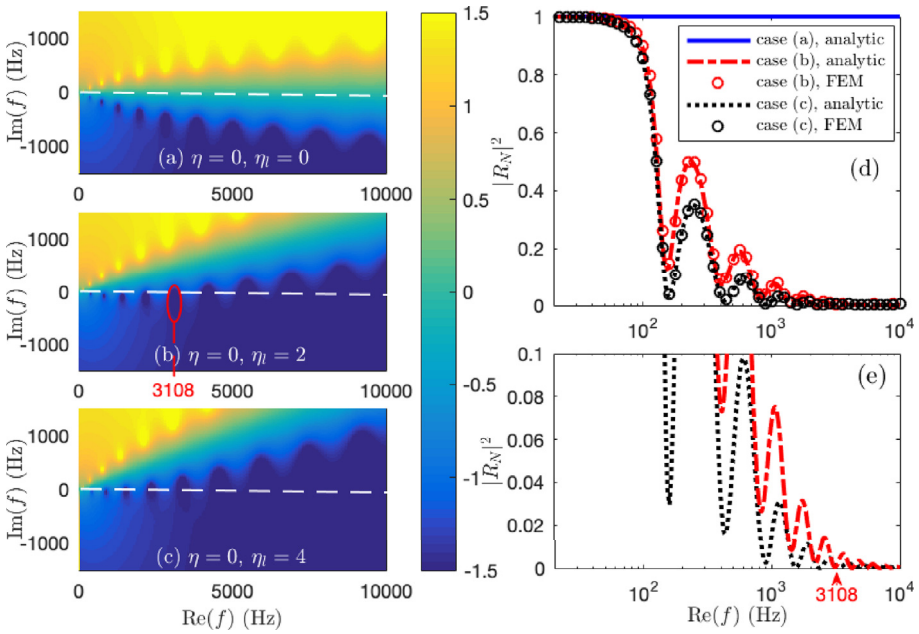

Fig. 3. (a)–(c) Representation of $\log_{10}(|R_N|)$ in the complex frequency plane for different loss factor values of the beam η and the viscous layer η_l. (d) Blue continuous, red dash-dotted and black dotted lines show the analytical reflection coefficient according to the real frequency for the configuration of (a),(b) and (c) respectively. Black and red circles show the numerical validations of configuration (b) and (c) respectively. (e) Zoom of the analytical curves of (d). (For interpretation of the references to color in this figure legend, the reader is referred to the Web version of this article.)

the opposite half space of the poles and there is a lack of loss, or the zeros are located in the same half space as the poles and there is an excess of loss. When the amount of losses exactly compensates the leakage of the system, the corresponding zero of the reflection coefficient is located on the real frequency axis, e.g. at Re(f) = 3108 Hz in Fig. 3(b). This situation is known as the critical coupling condition [15] and implies the impedance matching between the main beam and the resonator, leading to a perfect absorption of the incident wave at this specific real frequency (see Fig. 3(d)). A good agreement between the analytical and numerical results can also be observed in Fig. 3(d), therefore validating the analytical model presented in the previous sections.

An overlapping of the zeros on the real frequency axis is observed in Fig. 3(b) above the frequency at which the coupling condition is satisfied (Re(f) = 3108 Hz). This is due to the geometry of the resonator that leads to resonances with low quality factors. The overlapping of the wide zeros results in a broadband quasi-perfect absorption and $|R_N|^2 \simeq 0$ in this frequency range (see Fig. 3(d)). This result is one interpretation of the ABH effect at high frequency and is the main contribution of this work. The damping effect of a truncated ABH is the consequence of the critical coupling at one resonance frequency of the ABH and the broadband quasi-perfect absorption at higher frequencies. The critical coupling, and as a consequence the ABH effect of a truncated ABH, can be obtained for any power law of thickness profiles, provided that the impedance matching between the main beam and the ABH is achieved by compensating the energy leakage with additional dissipative losses from the viscoelastic layer. However, it is difficult to compensate the leakage with realistic materials for profiles with $\chi < 2$ due to the fact that the poles and zeros are far from the real frequency axis in the complex frequency plane, as demonstrated by Fig. 2(a). In practice, the critical coupling is therefore difficult to attain for such a profile type. For practical application, one interesting goal is to design a system that is critically coupled at the lowest resonance frequency as possible. However, this may require a significant amount of losses, therefore increasing the mass of the system, possibly destroying the higher frequency efficiency. Other strategies should therefore be developed.

4. Enhancement of the absorption of an ABH termination

This section proposes methods to enhance the absorption performance of an ABH termination. These methods are based on the use of the complex frequency plane, and can also be applied to any geometry termination. Two methods are presented. The first one is based on the spatial distribution of the losses introduced by the coating layer by gradually changing its thickness, i.e. h_j^l also varies with $h_j, j = 0, \dots, N-1$. The second method consists in slightly modifying the geometry of the ABH, by adding a mass at its extremity. In this case, the critical coupling at the first zero of the termination may be obtained, leading to a perfect absorption at low frequency.

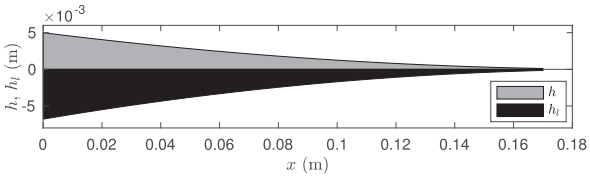

Fig. 4. Thickness profile of the ABH termination (grey) and the coating layer (black).

4.1. Tuning the losses introduced by the coating layer

An enhancement of the absorption properties of an ABH is proposed by tuning the distribution of losses along the ABH termination. Except for the thickness of the coating layer, the geometric and material parameters of the ABH and the coating layer remain the same in this section as in the previous sections (see Table 1). The thickness profile of the coating layer is shaped so that the losses introduced in the system efficiently compensate the leakage for each resonance of the termination, producing a broadband absorption. The progressive variation of losses is based on a similar phenomenon to graded materials [28]. The incoming wave reduces its speed progressively as it propagates through the ABH. The thickness of the coating layer (and thus the amount of losses) is tapered in such a way that the losses are higher where the wave travels faster. The thickness profile of the coating layer therefore decreases as well as the thickness profile of the beam as depicted in Fig. 4. This is defined as:

$$h_l(x) = 1.36 \times h_0 \left(\frac{x}{L_t} \right)^2, \forall x > L_0. \tag{10}$$

Fig. 5(a)-(b) show the reflection coefficient of the ABH and the coating layer described in Fig. 4 in the complex frequency plane in the lossless ($\eta = 0, \eta_l = 0$) and lossy ($\eta = 0, \eta_l = 2$) cases respectively. As the losses are introduced, the set of zeros are aligned on the real frequency axis. The critical coupling is therefore performed for each resonance frequency in the analysed frequency band, leading to a total absorption of flexural waves at these particular frequencies. To compare, Fig. 5(c)–(d) depict the reflection coefficient of the ABH with a coating layer of constant thickness $h_l = 4.7$ mm in the complex frequency plane in the lossless ($\eta = 0, \eta_l = 0$) and the lossy cases ($\eta = 0, \eta_l = 2$) respectively. Both configurations are designed in such a way that they provide the same absorption performance at the first resonance frequency $f_0 = 185.2$ Hz of the termination in the lossy case. It is worth noting that the quality factor and the density of poles depend on the profile of the coating layer: the

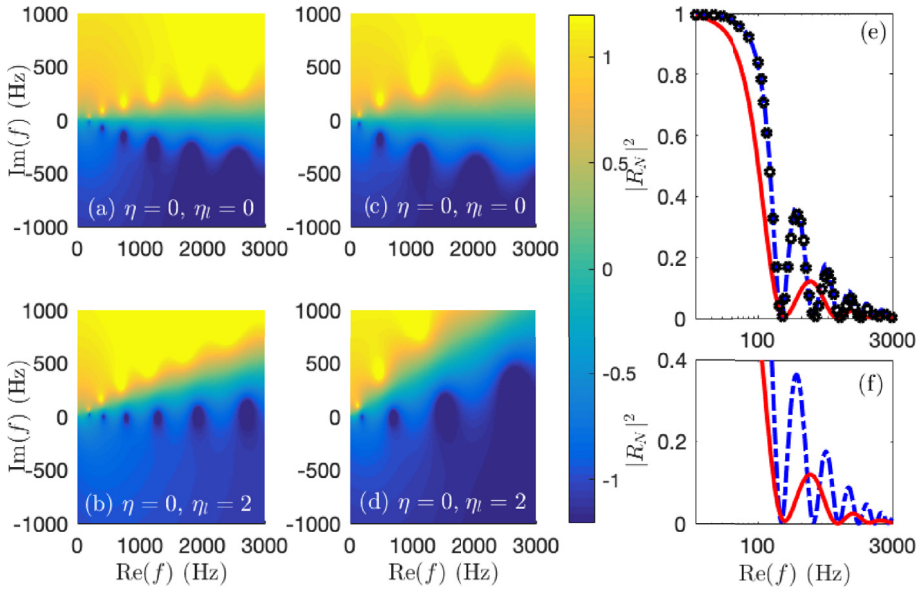

Fig. 5. (a)–(b) Representation of $\log_{10}(|R_N|)$ of the ABH with the profiled coating layer in the complex frequency plane for the lossless ($\eta = 0, \eta_l = 0$) and lossy ($\eta = 0, \eta_l = 2$) cases respectively. (c)–(d) Representation of $\log_{10}(|R_N|)$ of the ABH with a coating layer of constant thickness ($h_l = 4.7$ mm) in the complex frequency plane for the lossless ($\eta = 0, \eta_l = 0$) and lossy ($\eta = 0, \eta_l = 2$) cases respectively. (e) The blue dash-dotted line and black circles show the reflection coefficient of the ABH with a profiled coating layer according to the real frequencies using the analytical and numerical models, respectively. Red line shows the analytical reflection coefficient of the ABH with a coating layer of constant thickness ($h_l = 4.7$ mm). (f) Zoom of the analytical curves of (e). (For interpretation of the references to color in this figure legend, the reader is referred to the Web version of this article.)

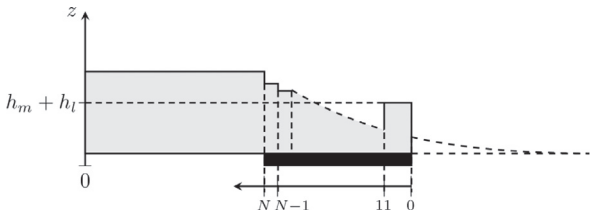

Fig. 6. Diagram of the spatial discretisation of the ABH with an added mass.

uniform coating layer provides a smaller density of poles than the profiled one, as well as a smaller quality factors of poles (see Fig. 5 (b) and (d)).

As opposed to the profiled case, the control of the position of a given zero in the uniform case cannot be achieved independently from the others. This is due to the fact that the losses introduced in the model are frequency independent, and that the thickness of the coating layer and η_l are constant in this case (see Fig. 5(c)–(d)). As a result, the distribution of zeros for $\mathrm{Re}(f) > f_0$ is not perfectly aligned on the real frequency axis in the presence of a coating layer of constant thickness (see the position of the fourth zero in Fig. 5(d)). This result highlights the relevance of using profiled coatings to control the position of the zeros independently from the others, and so to produce a cascade of perfect absorption peaks. The reflection coefficients of these two types of ABH terminations are shown in Fig. 5(e). The profiled case shows several falls of $|R_N|^2$ corresponding to perfect absorptions. However, the uniform profile has wider peaks due to the lower quality factor of the poles of $|R_N|^2$. The analytical results of the ABH with the profiled coating layer in Fig. 5(e) (blue dash-dotted line) are compared with numerical results (black circles). A good agreement between both results is noticed.

4.2. ABH termination with an added mass

Another parametric analysis based on the complex frequency plane is proposed to improve the absorbing performance of the ABH at low frequencies. The study is carried out by modifying the geometry of the ABH. In particular, a mass is added at the termination end with a varying thickness. The thickness h_m of the mass varies from 0.2 mm to 5 mm. The termination + beam system is still discretised by $N = 201$ beams and the mass consists of increasing the thickness of the 11 first beams of the termination (see Fig. 6). The geometric and material parameters of the ABH and the coating layer remain the same as in the

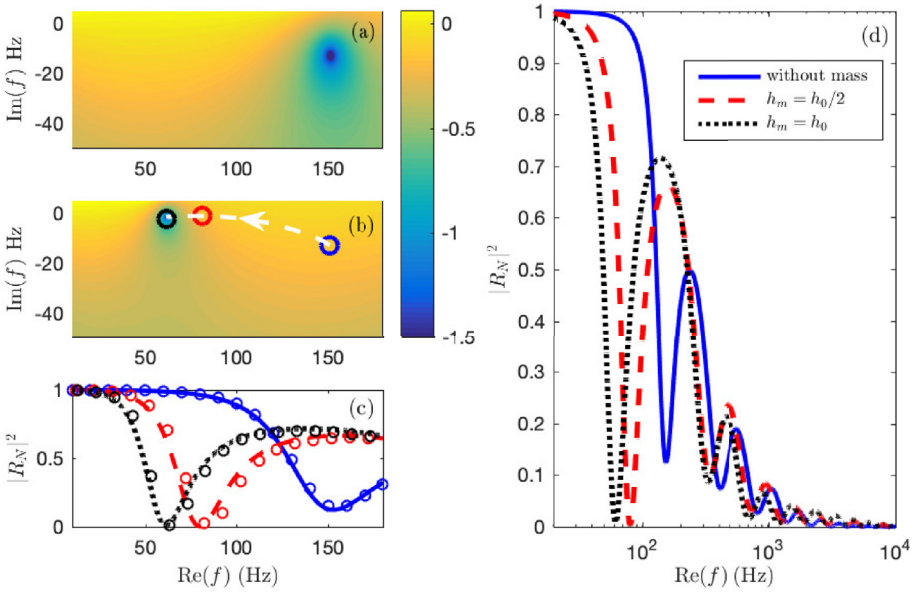

Fig. 7. (a) Representation of $\log_{10}(|R_N|)$ for the ABH in the complex frequency plane around its first zero. (b) Representation of $\log_{10}(|R_N|)$ in the complex frequency plane around its first zero in the case with an added mass of thickness $h_m = h_N$. White dashed line corresponds to the path of the zero when the thickness of the mass is increased. Blue, red and black circles give the positions of the zero for the configurations ABH, without mass, $h_m = h_N/2$ and $h_m = h_N$ respectively. (c) Blue continuous, red dashed and black dotted lines show the analytical reflection coefficient around the first real resonance frequency for the configurations shown with circles of same color in (b). Blue, red and black circles show the numerical validations. (d) Blue continuous, red dashed and black dotted lines show the analytical reflection coefficient according to the real frequency for the configurations shown with circles of same color in (b). (For interpretation of the references to color in this figure legend, the reader is referred to the Web version of this article.)

previous section and are described in Table 1. The lossy case is considered here and $\eta = 0$ and $\eta_l = 2$.

Fig. 7(a) depicts the reflection coefficient around its first zero in the complex frequency plane for an ABH configuration without added mass. The path of the zero in the complex frequency plane is also depicted according to the increase of the mass thickness in Fig. 7(b). As the mass thickness increases, the added mass effect in the termination increases too and the real frequency of the zero decreases. Moreover, the zero moves to the real frequency axis as the mass thickness increases. This is due to a localisation of the mode in the termination, leading to a decrease in leakage and thus a decrease in the absolute value of the imaginary frequency of the zero. In particular, the zero of the reflection coefficient is located on the real frequency axis starting from $h_m = h_N/2$. The critical coupling is therefore obtained and a perfect absorption of the incident wave is observed at $\mathrm{Re}(f) = 80$ Hz and $\mathrm{Re}(f) = 61.5$ Hz for $h_m = h_N/2$ and $h_m = h_N$ respectively (see Fig. 7(c)). The analytical results of Fig. 7(c) (black dotted, red dashed and blue line) are validated with numerical results (black, red and blue circles), since a good agreement is observed between both models. It is worth noting that the addition of mass does not deteriorate the absorbing properties of the ABH at high frequencies as seen in Fig. 7(d). These results highlight the possibility to improve the absorption efficiency of a 1D termination by modifying its geometry and by analysing the position of the zeros of its reflection coefficient in the complex frequency plane.

5. Conclusions

Absorption of propagative flexural waves by means of a 1D ABH termination is analysed in this work in the case of a reflection problem. The ABH effect is interpreted through the use of the complex frequency plane. The positions of the zeros of the eigenvalues of the scattering matrix in the complex frequency plane provide information on the absorption properties of the ABH. The ABH effect may be interpreted as a consequence of the critical coupling at one resonance frequency of the ABH and of the broadband quasi-perfect absorption at higher frequencies, thanks to the specific geometry of the resonator. This point is the main conclusion of the work since it provides a physical explanation of the ABH efficiency. The understanding of this mechanism provides the key to the optimisation procedure of an absorbing termination. Two methods are proposed to improve the absorption of a 1D ABH. The first consists in tuning the losses introduced in the system by shaping the thickness profile of the coating layer. In doing so it is possible to control the losses introduced in the resonator according to the real frequency. The second method relies on the addition of a mass at the end of the ABH. The configuration of perfect absorption at the first resonance frequency of the resonator can be obtained and controlled according to the added mass by controlling the position of the corresponding zero in the complex frequency plane.

Acknowledgements

This work has been funded by the RFI Le Mans Acoustic (Région Pays de la Loire) within the framework of the Metaplaque project. This article is based on work from COST action DENORMS CA 15125, supported by COST (European Cooperation in Science and Technology). This work was partly supported by the Spanish Ministry of Economy and Innovation (MINECO), by the European Union FEDER through project FIS2015-65998-C2-2, by the project AICO/2016/060 by Consellería de Educación, Investigación, Cultura y Deporte de la Generalitat Valenciana and by the project eTNAA ANR-17-CE08-0035-01 (projet ANR 2017–2010).

References

[1] D. Ross, E. Ungar, E. Kerwin, Damping of plate flexural vibrations by means of viscoelastic laminae, Structural damping (1960) 49–87.
[2] M. Mironov, Propagation of a flexural wave in a plate whose thickness decreases smoothly to zero in a finite interval, Soviet Physics Acoustics-USSR 34 (3) (1988) 318–319.
[3] J.Y. Lee, W. Jeon, Vibration damping using a spiral acoustic black hole, J. Acoust. Soc. Am. 141 (3) (2017) 1437–1445.
[4] T. Zhou, L. Tang, H. Ji, J. Qiu, L. Cheng, Dynamic and static properties of double-layered compound acoustic black hole structures, International Journal of Applied Mechanics 9 (2017) 1750074 (05).
[5] T. Zhou, L. Cheng, A resonant beam damper tailored with acoustic black hole features for broadband vibration reduction, J. Sound Vib. 430 (2018) 174–184.
[6] A. Climente, D. Torrent, J. Snchez-Dehesa, Omnidirectional broadband insulating device for flexural waves in thin plates, J. Appl. Phys. 114 (21) (2013) 214903.
[7] A. Climente, D. Torrent, J. Snchez-Dehesa, Gradient index lenses for flexural waves based on thickness variations, Appl. Phys. Lett. 105 (6) (2014) 064101.
[8] H. Zhu, F. Semperlotti, Two-dimensional structure-embedded acoustic lenses based on periodic acoustic black holes, J. Appl. Phys. 122 (6) (2017) 065104.
[9] L. Tang, L. Cheng, Enhanced acoustic black hole effect in beams with a modified thickness profile and extended platform, J. Sound Vib. 391 (2017) 116–126.
[10] J. Deng, L. Zheng, P. Zeng, Y. Zuo, O. Guasch, Passive constrained viscoelastic layers to improve the efficiency of truncated acoustic black holes in beams, Mech. Syst. Signal Process. 118 (2019) 461–476.
[11] V. Denis, A. Pelat, C. Touz, F. Gautier, Improvement of the acoustic black hole effect by using energy transfer due to geometric nonlinearity, Int. J. Non-Linear Mech. 94 (2017) 134–145.
[12] H. Li, C. Touz, A. Pelat, F. Gautier, X. Kong, A vibro-impact acoustic black hole for passive damping of flexural beam vibrations, J. Sound Vib. 450 (2019) 28–46.
[13] V. Romero-Garca, G. Theocharis, O. Richoux, V. Pagneux, Use of complex frequency plane to design broadband and sub-wavelength absorbers, J. Acoust. Soc. Am. 139 (6) (2016) 3395–3403.
[14] J. Leng, F. Gautier, A. Pelat, R. Pic, J.-P. Groby, V. Romero-Garca, Limits of flexural wave absorption by open lossy resonators: reflection and transmission problems, New J. Phys. 21 (053003).
[15] A. Yariv, Universal relations for coupling of optical power between microresonators and dielectric waveguides, Electron. Lett. 36 (4) (2000) 321–322.
[16] J.R. Piper, S. Fan, Total absorption in a graphene monolayer in the optical regime by critical coupling with a photonic crystal guided resonance, ACS Photonics 1 (4) (2014) 347–353.

[17] N. Jimnez, V. Romero-Garca, V. Pagneux, J.-P. Groby, Rainbow-trapping absorbers: broadband, perfect and asymmetric sound absorption by subwavelength panels for transmission problems, Sci. Rep. 7 (1) (2017) 13595.
[18] J.-P. Groby, R. Pommier, Y. Aurgan, Use of slow sound to design perfect and broadband passive sound absorbing materials, J. Acoust. Soc. Am. 139 (4) (2016) 1660–1671.
[19] V. Krylov, F. Tilman, Acoustic black holes for flexural waves as effective vibration dampers, J. Sound Vib. 274 (35) (2004) 605–619.
[20] V.V. Krylov, R. Winward, Experimental investigation of the acoustic black hole effect for flexural waves in tapered plates, J. Sound Vib. 300 (12) (2007) 43–49.
[21] V. Denis, F. Gautier, A. Pelat, J. Poittevin, Measurement and modelling of the reflection coefficient of an acoustic black hole termination, J. Sound Vib. 349 (2015) 67–79.
[22] V. Georgiev, J. Cuenca, F. Gautier, L. Simon, V. Krylov, Damping of structural vibrations in beams and elliptical plates using the acoustic black hole effect, J. Sound Vib. 330 (11) (2011) 2497–2508.
[23] V. Denis, A. Pelat, F. Gautier, Scattering effects induced by imperfections on an acoustic black hole placed at a structural waveguide termination, J. Sound Vib. 362 (2016) 56–71.
[24] V. Denis, A. Pelat, F. Gautier, B. Elie, Modal overlap factor of a beam with an acoustic black hole termination, J. Sound Vib. 333 (12) (2014) 2475–2488.
[25] P.A. Feurtado, S.C. Conlon, Investigation of boundary-taper reflection for acoustic black hole design, Noise Control Eng. J. 63 (5) (2015) 460.
[26] L. Tang, L. Cheng, H. Ji, J. Qiu, Characterization of acoustic black hole effect using a one-dimensional fully-coupled and wavelet-decomposed semi-analytical model, J. Sound Vib. 374 (2016) 172–184.
[27] B. Mace, Wave reflection and transmission in beams, J. Sound Vib. 97 (2) (1984) 237–246.
[28] C. Vemula, A. Norris, G. Cody, Attenuation of waves in plates and bars using a graded impedance interface at edges, J. Sound Vib. 196 (1) (1996) 107–127.